Crossed-beam experiment for the scattering of low- and intermediate-energy electrons from BF3: A comparative study with XF3 (X = C, N, and CH) molecules

M. Hoshino, P. Limão-Vieira, A. Suga, H. Kato, F. Ferreira da Silva, F. Blanco, G. García, and H. Tanaka

Citation: The Journal of Chemical Physics **143**, 024313 (2015); doi: 10.1063/1.4926539

View online: http://dx.doi.org/10.1063/1.4926539

View Table of Contents: http://scitation.aip.org/content/aip/journal/jcp/143/2?ver=pdfcov

Published by the AIP Publishing

Crossed-beam experiment for the scattering of low- and intermediate-energy electrons from BF_3: A comparative study with XF_3 (X = C, N, and CH) molecules

M. Hoshino,[1,a)] P. Limão-Vieira,[1,2] A. Suga,[1] H. Kato,[1] F. Ferreira da Silva,[2] F. Blanco,[3] G. García,[4] and H. Tanaka[1]

[1]*Department of Physics, Sophia University, Tokyo 102-8554, Japan*
[2]*Laboratório de Colisões Atómicas e Moleculares, CEFITEC, Departamento de Física, Faculdade de Ciências e Tecnologia, Universidade Nova de Lisboa, 2829-516 Caparica, Portugal*
[3]*Departamento de Fisica Atomica, Molecular y Nuclear, Facultad de Ciencias Fisicas, Universidad Complutense de Madrid, E-28040 Madrid, Spain*
[4]*Instituto de Fisica Fundamental, Consejo Superior de Investigaciones Científicas, 28006 Madrid, Spain*

(Received 25 May 2015; accepted 29 June 2015; published online 14 July 2015)

Absolute differential cross sections (DCSs) for electron interaction with BF_3 molecules have been measured in the impact energy range of 1.5–200 eV and recorded over a scattering angle range of 15°–150°. These angular distributions have been normalized by reference to the elastic DCSs of the He atom and integrated by employing a modified phase shift analysis procedure to generate integral cross sections (ICSs) and momentum transfer cross sections (MTCSs). The calculations of DCSs and ICSs have been carried out using an independent atom model under the screening corrected additivity rule (IAM-SCAR). The present elastic DCSs have been found to agree well with the results of IAM-SCAR calculation above 20 eV, and also with a recent Schwinger multichannel calculation below 30 eV. Furthermore, in the comparison with the XF_3 (X = B, C, N, and CH) molecules, the elastic DCSs reveal a similar angular distribution which are approximately equal in magnitude from 30 to 200 eV. This feature suggests that the elastic scattering is dominated virtually by the 3-outer fluorine atoms surrounding the XF_3 molecules. The vibrational DCSs have also been obtained in the energy range of 1.5–15 eV and vibrational analysis based on the angular correlation theory has been carried out to explain the nature of the shape resonances. Limited experiments on vibrational inelastic scattering confirmed the existence of a shape resonance with a peak at 3.8 eV, which is also observed in the vibrational ICS. Finally, the estimated elastic ICSs, MTCSs, as well as total cross sections are compared with the previous cross section data available. © *2015 AIP Publishing LLC.* [http://dx.doi.org/10.1063/1.4926539]

I. INTRODUCTION

Halogen-containing compounds such as gaseous BF_3 have been widely used in the plasma-assisted fabrication of large integrated circuits, semiconductor fabrication, surface hardening, and other technological applications. Recently, BF_3 has been suggested as a replacement molecule for diborane, B_2H_6 used as a p-type dopant of amorphous silicon films in solar cells.[1] In order to perform plasma discharge simulations as accurately as possible, reliable low-energy electron collision cross sectional data are needed. Recently, calculations on the collisional cross sections for scattering of F^+, B^+, BF^+, and BF_2^+ ions from BF_3 have been reported.[2] A consistent set of low-energy electron collision cross sections has also been derived from the measured electron transport coefficients for a pure BF_3 molecule using an electron swarm study and a two-term approximation of the Boltzmann equation for energy.[1]

To our knowledge, the previous work on electron interactions with BF_3 includes ionization cross sections,[3–5] dissociative electron attachments,[6–8] grand total cross section (TCS) measured by Szmytkowski *et al.*,[9] and calculated ionization and TCS with an independent atom model by Vinodkumar *et al.*[10] Angular differential-vibrational excitation of BF_3 for symmetry stretching v_1 and degenerate stretching v_3 modes were reported as a function of the electron energy with a crossed-beam method by Tronc *et al.*[11] As far as elastic differential cross sections (DCSs) and integral cross sections (ICSs) are concerned, we note a few theoretical studies on multi-scattering Xα-calculation of the unoccupied a''_2, a'_1, and e' molecular orbitals of BF_3 and BCl_3 by Tossel *et al.*[12] which are compared with electron transmission spectroscopy (ETS) measurements as well as R-matrix calculations by Radmilović-Radjenović[13] on the elastic scattering and electronic excitation of BF_3 by low energy electrons. More recently, the Schwinger multichannel (SMC) method was employed in the static-exchange (SE) and the static-exchange-polarization (SEP) approximations in the energy range from 0.1 to 10 eV.[14,15] However, no systematic measurement of the DCS has been reported in a wider electron energy region from low- to intermediate-energy range. The present study, therefore, represents a new and original experimental contribution of the DCS data

a)Author to whom correspondence should be addressed. Electronic mail: masami-h@sophia.ac.jp. Tel: (+81) 3 3238 4227. Fax: (+81) 3 3238-3341.

for BF_3 in the energy range of 1.5–200 eV, which have been compared with similar 3-fluorine atom compounds on elastic-scattering from NF_3,[16–18] CHF_3,[19] and CF_3-radical.[20,21] These results are also compared with the optical potential calculations assuming an independent atom model under the screening corrected additivity rule (IAM-SCAR) but including screening corrections in order to account for the molecular geometries.[22,23]

In a recent work on the elastic scattering from the halomethane-molecules, CH_3F, CH_3Cl, CH_3Br, and CH_3I,[24] we have shown for the first time atomic-like behavior of these scattering systems by comparing the elastic DCSs of these molecules with those for the corresponding noble gases, Ne, Ar, Kr, and Xe, respectively. Such behavior was soon after shown for other molecular systems as CCl_4,[25] SiF_4,[26] GeF_4,[27] COS and CS_2,[28] and C_4F_6 isomers[29] scattering systems by comparison of the elastic DCSs for corresponding atomic chlorine, fluorine, and sulphur atoms in the intermediate impact energy region, respectively. Here, we also verify, for the first time, such atomic-like behavior in the electron scattering processes from XF_3 (X = B, C, N, and CH) molecules.

In Sec. II, we provide details on the experimental apparatus and procedures that have been used in the present work. In Sec. III, we present a brief description on the calculation and extrapolation methods for the DCSs and in Sec. IV, the experimental data are presented together with a discussion and comparison with other experimental and theoretical results. Finally, some conclusions that can be drawn from this study are given in Sec. V.

II. EXPERIMENTAL DETAILS

The two electron spectrometers used in the present work have been described thoroughly in previous publications (e.g., Tanaka *et al.*[30,31] and Kato *et al.*,[24] respectively). Generally speaking, both spectrometers employed are identical apparatus except for the following arrangements. In the latter setup, scattering angles are covered from −20° to 150°, with the electron monochromator differentially pumped. The overall energy resolution is set to approximately 35 meV and 100 meV (FWHM), for electron impact energies of 1.5–30 eV in the former and for 50–200 eV in the latter experimental setup, respectively. However, lower vibrational modes of BF_3,[32] ν_4 (59 meV), ν_2 (86 meV), ν_1 (110 meV), and ν_3 (180 meV) are excited together with rotational excitation contributions to the elastic peak. Within the present resolution, these can be observed as the two distinctive groups of bands attributable to the composed ($\nu_4 + \nu_2 + \nu_1$) modes and degenerate stretching (ν_3) mode as shown in Fig. 1. In general, vibrational excitation contributes to about a few percent at higher impact energies (above 30 eV), with little influence on the shape of the elastic peak. However, around the Ramsauer-Townsend (R-T) minimum expected at 1.5 eV,[15] a symmetric stretching vibration (ν_3) is normally expected to exceed the elastic cross section. Moreover, both elastic and vibrational excitations are normally enhanced around the shape resonance at 3.8 eV.[9]

The energy scale was also calibrated by reference to He ^2S Feshbach-resonance at 19.37 eV and the first peak of $\nu = 0 \rightarrow 1$ excitation in the $^2\Pi_g$ shape resonance in N_2

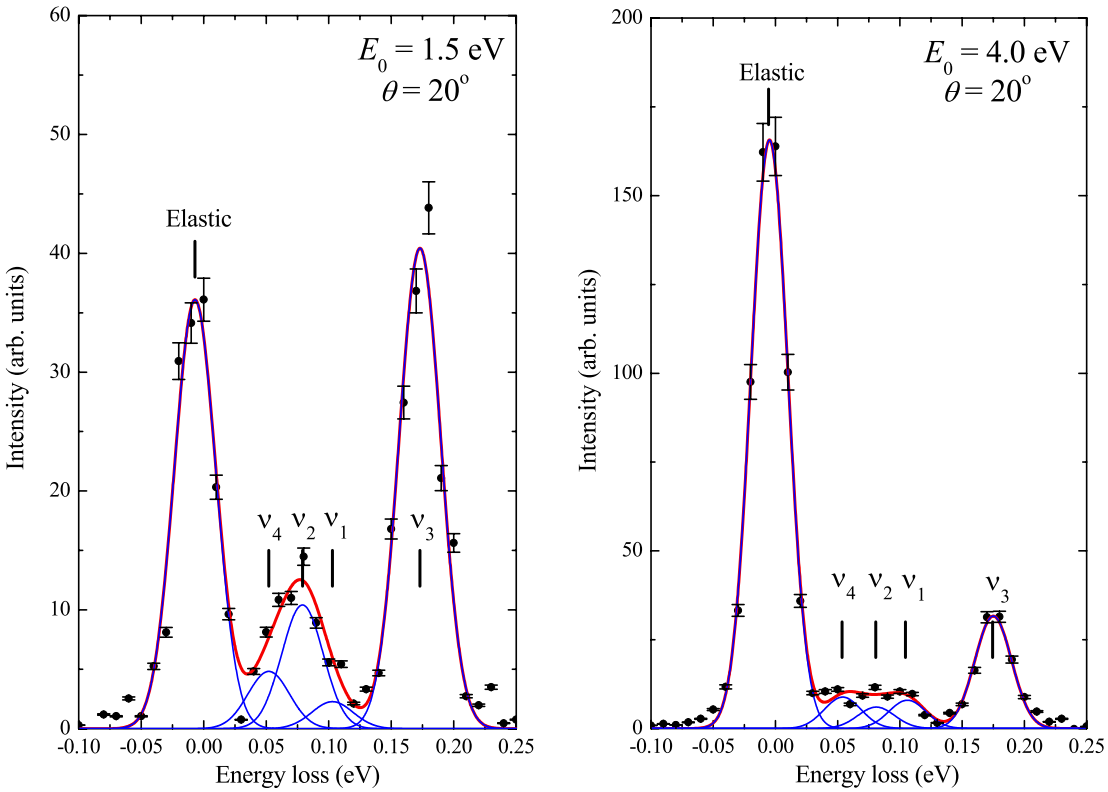

FIG. 1. Typical energy loss spectra of scattered electrons from BF_3 at an impact energy of 1.5 eV and 4 eV, and at a scattering angle of 20°. The elastic peak and low-lying vibrational-modes, v_1 (0.110 eV), v_2 (0.086 eV), v_3 (0.180 eV), and v_4 (0.059 eV),[32] are shown by bar plots.

at an incident energy of 1.97 eV.[33] In both setups, the angular scale and their resolution within ±1.5° were determined from the symmetry in the intensity profile of the He 2^1P inelastic transition measured by changing the scattering angle of $\pm\theta$ against the nominal-scattering angle at 0°. The molecular beam was produced effusively from a nozzle with the length of 5-mm and diameter of 0.3-mm, kept at slightly elevated temperatures (50–70 °C) throughout the measurements to avoid nozzle surface contamination by BF_3.

The observed counts of the scattered electrons were converted into absolute cross sections by re-measurements of the well-known DCSs of He[34] using the well-established relative flow technique.[35–39] That calibration requires constant Knudsen numbers for BF_3 and He to generate equal two gas densities in the collision volume, for which the head pressures behind the nozzle were about 0.5 Torr for BF_3 (4.90 Å) and 2.5 Torr for He (2.18 Å). Those were estimated based on the hard sphere model.

In a single hemispherical analyzer without real slits (virtual slits), some electrons with energies higher than passing energy, E_0 of the analyzer are reflected from the walls,[40] leading to the long tail on the energy-loss side of the elastic peak (about 3% or less of the elastic peak). With the present energy resolution, the v_4-vibrational mode (59 meV) cannot be resolved completely from the elastic peak which can be represented rather well by the sum of a Gaussian peak (height ≈3%) plus a very broad Lorentz function. However, the vibrational peaks in the energy loss spectra were estimated through a Gaussian fitting procedure to distinguish them from the background signal. Experimental errors are estimated as 10%–15% for elastic DCSs, ~25% for inelastic vibrational DCSs, and 30%–33% for ICSs and momentum transfer cross sections (MTCSs).

III. THEORETICAL APPROACH, FITTING, AND INTEGRATION METHOD

Details of the application of the IAM-SCAR[22,23] method to electron interactions have been provided in a number of previous papers (see, e.g., Refs. 25–29). Briefly, each atomic target (B, F) is represented by an interacting complex potential (the so-called optical potential). The real part accounts for the elastic scattering of the incident electrons, and the imaginary part represents the inelastic processes, which are considered as "absorption" from the incident beam. For the elastic part, the potential is represented by the sum of three terms: (a) a static term derived from a Hartree-Fock calculation of the atomic charge density distribution, (b) an exchange term to account for the indistinguishability of the incident and target electrons, and (c) a polarization term for the long-range interactions which depends on the target polarizability. The inelastic scattering, on the other hand, is treated as electron-electron collisions. Further improvements to the original formulation in the description of the electron's indistinguishability and the inclusion of screening effects led to a model which provides a good approximation for electron-atom scattering over a broad energy range. To calculate the cross sections for electron collisions with BF_3, the additivity rule (AR) is then applied to the optical model results for each constituent atom. In this approach, the molecular scattering amplitude stems from the coherent sum of all the relevant atomic amplitudes, which gives the DCSs for the molecule of interest. ICSs can then be determined by integrating those DCSs. The geometry of the molecule (atomic positions and bond lengths) is taken into account by using some screening coefficients and this enables the range of validity of the technique to be extended down to impact energies of ~30 eV (or lower) for electron scattering.

In order to obtain the experimental ICSs and MTCSs, the integrations were carried out as follows. The measured elastic DCSs were extrapolated ($\theta < 15°$ and $\theta > 150°$) with a modified phase shift analysis (MPSA), including polarization and the Born approximation for the higher phase shifts,[41] or the corresponding shapes of our IAM-SCAR calculation as a guide (see, e.g., Refs. 25–29 and references therein for details on the calculation procedure). The DCS, $\frac{d\sigma}{d\Omega} = |f(\theta)|^2$, is defined in terms of the scattering amplitude as

$$f(\theta) = \frac{N_k}{2iK}\left[\sum_{l=0}^{L}\left[S_l(k)-1\right](2l+1)\,P_l(\cos\theta)+C_L(k,\alpha,\theta)\right],$$

with

$$C_L(k,\alpha,\theta) = 2i\pi\alpha k^2\left\{\frac{1}{3}-\frac{1}{2}\sin\frac{\theta}{2} - \sum_{l=1}^{L} P_l(\cos\theta)/(2l+3)(2l-1)\right\},$$

where k is the incident electron wave number, $S_l(k)$ is the scattering matrix, and N_k depends on the least square fitting procedure employed. In addition, $C_L(k,\alpha,\theta)$ is the Thompson's form of the Born approximation for higher phases,[42] and $\alpha = 3.31$ Å^3 (Ref. 43) is the polarizability of BF_3. Finally, the parameterized DCSs were numerically integrated by using

$$Q_I = 2\pi\int_0^{\pi}\frac{d\sigma}{d\Omega}\sin\theta d\theta$$

for ICSs and

$$Q_m = 2\pi\int_0^{\pi}\frac{d\sigma}{d\Omega}[1-\cos\theta]\sin\theta d\theta$$

for MTCS, respectively.

IV. RESULTS AND DISCUSSION

Figure 2 shows the absolute elastic DCSs of BF_3 at electron impact energies from 1.5 to 200 eV for scattering angles from 15° to 150° with the MPSA fittings (red chain curves from 1.5 to 20 eV) for the full angular range, i.e., from 0° to 180°. The calculated results from the present IAM-SCAR, recent SMC-SE,[14] and SMC-SEP[15] methods are also plotted from 1.5 to 200 eV in Fig. 2. In order to make a clear comparison between experiment and the theoretical methods, the angular behavior is illustrated separately in Figs. 3 and 4 for the DCSs of XF_3 (X = B, C, N, and CH) at intermediate- and high-electron impact energies. The typical electron energy loss (EEL) spectra at 1.5 eV, 20° and 4.0 eV, 20° of BF_3 in the vibrational excitation were recorded with an apparatus resolution of 30–40 meV as shown in Fig. 1 and the angular

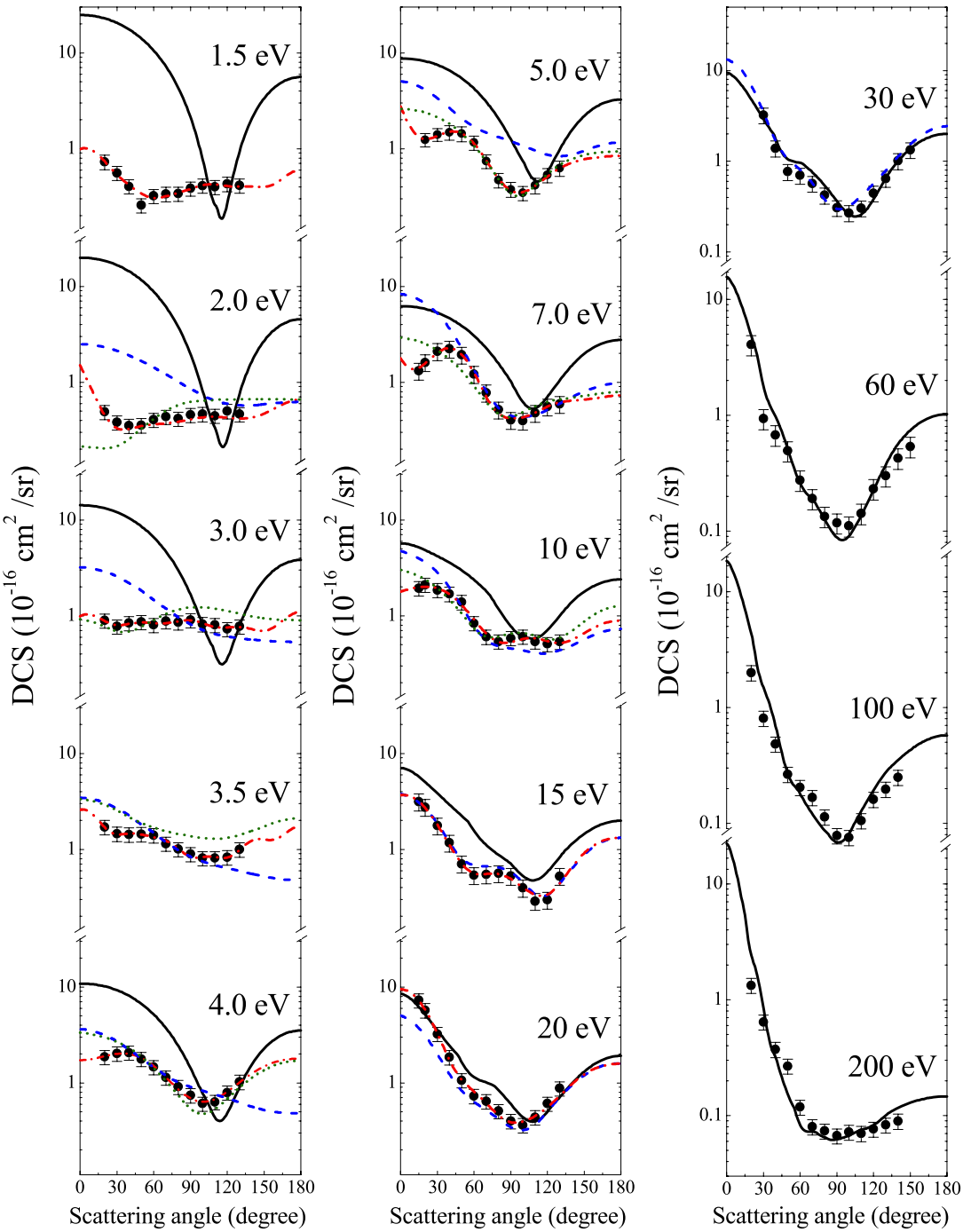

FIG. 2. Elastic differential cross sections (10^{-16} cm^2 sr^{-1}) for BF_3 at impact energies between 1.5 and 200 eV, together with present IAM-SCAR and previous theoretical calculations.[14,15] (●): present measurements, red dashed-dotted and black solid lines: present MPSA fitting and IAM-SCAR calculations, respectively. Blue dashed and green dotted lines: the SMC-SE and -SEP calculations,[15] respectively (see in text).

distributions of vibrational inelastic DCSs in Fig. 5 at the incident energies 1.5, 4.0, and 15 eV. Vibrational DCSs of resolved fundamental modes at 4.0 eV are also shown together with the fitting lines by a vibrational analysis in Fig. 6. Angular integrated cross sections for elastic and inelastic scatterings are presented together with total cross section available from the literature in Fig. 7.

All DCSs and their ICSs as well as MTCSs are tabulated as numerical data in Table I. Errors are estimated as follows: the He reference data are accurate to about 10%, the elastic DCS introduces another 10% statistical and systematic errors, giving a total of about 15%. Some physical properties of BF_3 are summarized in Table II.

A. Elastic DCS at 1.5–10 eV

The current elastic DCSs for BF_3 are shown in Fig. 2 together with the corresponding results from MPSA fitting in the impact energy range of 1.5–20 eV. The present IAM-SCAR calculations and recent SMC calculations[14,15] are also plotted. As shown in Fig. 2, we can distinguish three different electron energy regions. At low and intermediate energies,

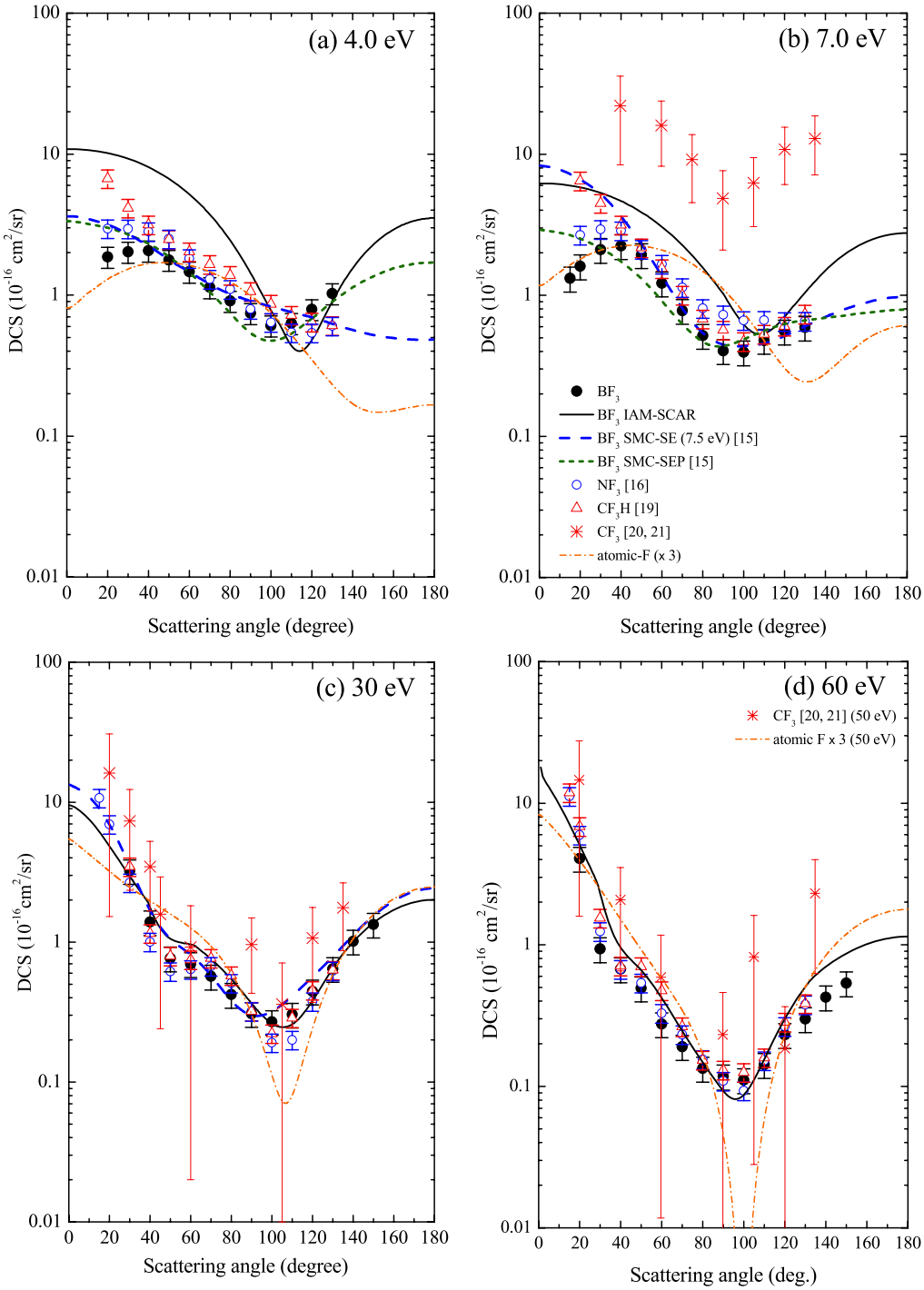

FIG. 3. Comparison of the present DCSs for BF_3 with the XF_3 (X = C,[20,21] N,[16] and CH[19]) molecules at (a) 4.0 eV, (b) 7.0 eV, (c) 30 eV, and (d) 60 eV (see legend for details).

i.e., 1.5–15 eV, the present DCSs can be compared with the recent SMC-SE and SMC-SEP calculations of da Costa *et al.*[14] and Pastega *et al.*,[15] respectively. From the latter study, a better agreement with the present experimental DCS in the electron energy range below 10 eV is obtained except for scattering angles smaller than 40°. Below 10 eV, the DCS decreases in magnitude as the scattering angle becomes smaller. However, forward scattering begins to slightly increase at 3.5 eV, where the angular distribution shows a relatively isotropic behavior. We note that a shape resonance has been reported at ~3.5 eV with B_2 symmetry of the C_{2v} group, corresponding to the A_2'' symmetry of the D_{3h} group as pointed out by Pastega *et al.*[15] Such behavior of the angular distribution has also been observed in the case of T_d symmetry molecules such as CCl_4[25] and CF_4[44] at electron impact energies near or above the energy position of the shape resonances. The R-T minimum at 0.7 eV in the A_1 state[15] is outside of the present impact energy region, but the effect can still be clearly observed in the isotropic behavior of the DCS below 3.5 eV, except for smaller scattering angles, i.e., below 40°. Such is reminiscent of *s*-wave ($l = 0$) scattering which dominates in the R-T minimum.

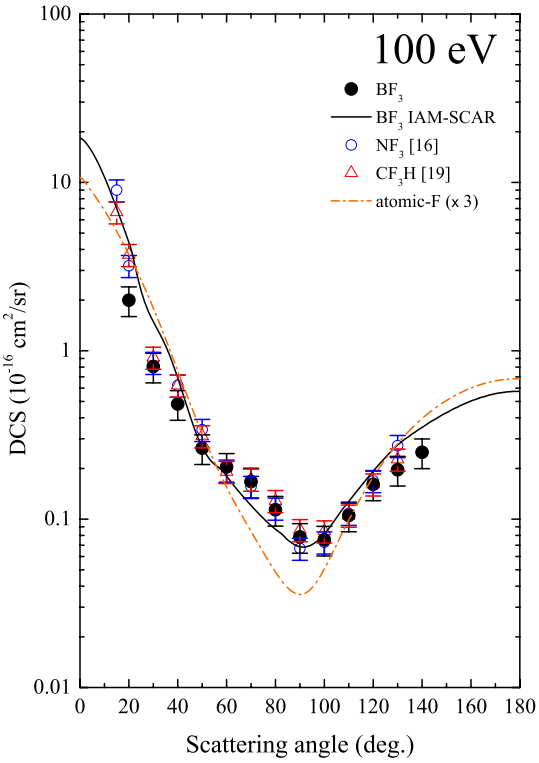

FIG. 4. Comparison of the present DCSs for BF_3 with the XF_3 (X = N[16] and CH[19]) molecules and the DCS calculated for atomic-fluorine at an impact energy of 100 eV, which is multiplied by factor of 3 in order to demonstrate the effect of three atomic-F in the target molecule.

B. Elastic DCS at 15–200 eV

Above 15 eV, we observe a very good agreement between the measured DCSs for BF_3 and the IAM-SCAR calculations with two minima discernible. One is a clear minimum at ~100°, which slightly shifts to larger scattering angles and becomes shallower at 200 eV, whereas the other is a less pronounced minimum close to 40°–50°at 15 eV, which progressively shifts to smaller scattering angles with increasing electron impact energies. Since BF_3 has no permanent dipole moment, we consider that the strong increase in the magnitude of the DCSs at forward scattering angles by long-range interaction (more noticeable at higher impact energies) is dictated by the relatively large value of BF_3 dipole polarizability (3.31 Å^3).[43]

C. Comparison in angular distribution with XF_3 and atomic-F DCSs

In Figs. 3(a)–3(d), we compare our elastic DCSs of BF_3 with those of XF_3 (X = C,[20,21] N,[16] and CH[19]) molecules together with the IAM-SCAR and the SMC calculations for BF_3 at 4.0, 7.0, 30, and 60 eV. At 4.0 eV, close to the resonance energy in the B_2 symmetry of C_{2v} group, the DCS for BF_3 has a minimum around 100° attributed to *p*-wave-like scattering as pointed out by Pastega *et al.*[15] It is interesting to note that NF_3 DCS shows a similar behavior as BF_3, whereas for CHF_3 it decreases monotonically with increasing scattering angle. At 7.0 eV and above 40°scattering angle, BF_3, NF_3, and CHF_3 show identical angular distributions. However, CF_3 radical DCS reported recently by Brunton *et al.*[20,21] appears

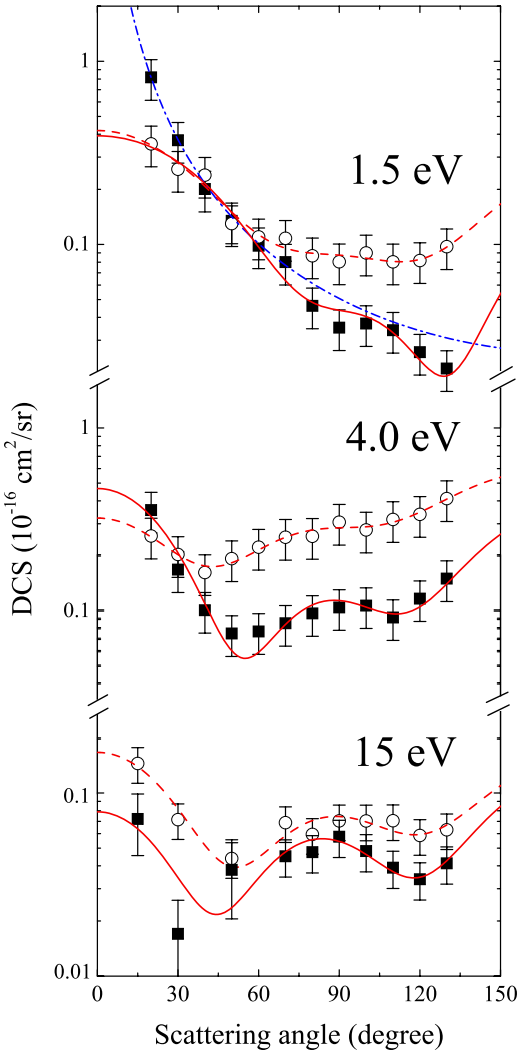

FIG. 5. Vibrational differential cross sections (10^{-16} cm^2 sr^{-1}) for BF_3 at energies of 1.5, 4.0, and 15 eV, corresponding to off-resonant and on-resonant energies, respectively. (■) and solid lines: present DCSs and fitting lines for the υ_3-degenerate stretching based on the vibrational analysis.[53,54] (○) and dashed-lines: for the ($\upsilon_1 + \upsilon_2 + \upsilon_4$) composed modes. Dotted-dashed line: Born approximation for υ_3 mode.[50]

one order of magnitude higher than BF_3, NF_3, and CHF_3 molecules albeit with similar DCS shape and local minimum at ~90°. The SMC calculations by Diniz *et al.*[45] have shown the similarity between the elastic DCSs of the CF_3 radical and CHF_3 molecules. Moreover, it also has reproduced well our previous experimental results[19] in the energy range of 6.5 eV–30 eV. This large discrepancy in the DCS magnitude at 7.0 eV (a factor of 10) cannot be explained neither from the worse energy resolution (~420 meV in the experiment[21]) nor from the enhancement due to a shape resonance even if emerged. The present result supports rather the theoretical calculations of CF_3 radical.[21,45,46] At 30 and 60 eV, the angular distributions of DCSs for XF_3 (X = B, N, and CH) molecules look like a further overlapped feature, whereas DCSs of CF_3 cannot be simply compared because of the large error bars. As discussed above, the IAM-SCAR calculations match perfectly well the experimental DCSs for energies above 30 eV.

In Fig. 4, we compare in detail the present results for BF_3 with previous measurements on NF_3 and CF_3H molecules

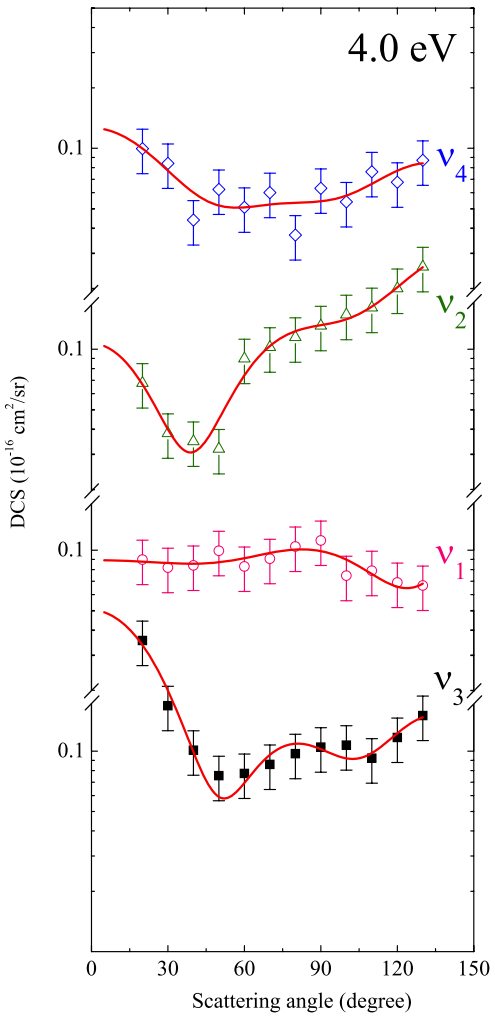

FIG. 6. Vibrational differential cross sections (10^{-16} cm^2 sr^{-1}) of resolved vibrational modes, v_1, v_2, v_3, and v_4 at an impact energy of 4.0 eV. (○), (△), (■), and (◊): vibrational DCSs of v_1, v_2, v_3, and v_4, respectively. Solid lines: fitting results by Legendre polynomials from the angular correlation theory.[53,54]

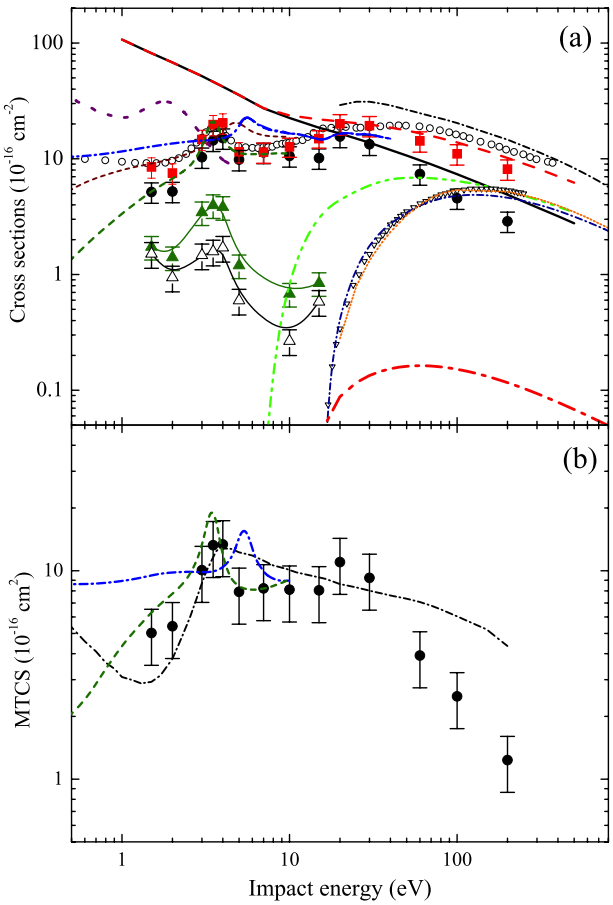

FIG. 7. The elastic (a) ICS, Q_I, vibrational ICS, TCS and (b) MTCS, Q_m for BF_3 derived from the present DCSs and compared with other previous experimental and theoretical results. (a) Elastic ICS—(●) and solid line (black): present results and the IAM-SCAR calculation, dotted-dashed line (blue): SMC-SE,[14,15] short-dashed line (green): SMC-SEP,[15] dotted-line (purple): Xα-calculation,[12] short-dashed line (wine): R-matrix calculation.[13] Inelastic ICS—(▲) (dark green) and (Δ) (black): present vibrational ICSs for ($v_1 + v_2 + v_4$) composed mode and v_3-degenerate stretching mode, respectively. Chain double-dashed line (green): total inelastic ICS in present IAM-SCAR calculation, (∇) (black),[3] dotted-dashed line (dark blue),[4] and dotted-line (orange):[10] ionization cross sections. Dashed-dotted line (red): BEf-scaled ICS for electronic excitation cross section to π^* state.[51] TCS—(■) and dashed line (red): present results and IAM-SCAR calculation. (○): experimental TCS,[9] dashed-dotted line (black): IAM calculation in Ref. 10. (b) (●): present results, dotted-dashed line (blue): SMC-SE,[14,15] short-dashed line (green): SMC-SEP,[15] thin dashed-dotted line (black): MTCS derived from swarm experiments.[2]

together with theoretical calculations for the fluorine atom at an impact energy of 100 eV. Note that the DCSs for atomic-F are multiplied by a factor of 3 in Figs. 3 and 4. The structure observed for BF_3 is well-reproduced in the IAM-SCAR calculation. This is due to "interference between single scattering centers" in multiple scattering with a single molecule. A deep minimum is observed at around 90°. Given that the IAM-SCAR theoretical approach is built upon scattering from atomic centers, from a qualitative point of view, the agreement between experimental DCSs for XF_3 molecules and calculated DCS for the F-atom is remarkably good. This is strong evidence in support of the assertion that atomic-like effects may remain prevalent in what are fundamentally molecular systems. As so, at these energies, the scattering process is dominated mainly by the outer atoms in the molecule, i.e., the incoming electron mainly sees the charge cloud distributions produced by the fluorine atoms surrounding the central boron, nitrogen, and carbon atoms, which mainly behave as spectators in the collision processes. Similar behavior has been observed for the case of CCl_4,[25] YF_4 (Y = C, Si, and Ge),[27] COS and CS_2,[28] and recently in C_nF_6 molecules (n = 2, 3, 4, and 6).[29] For these molecular systems, the central atoms are lighter than the outer atomic system. However, in the case of YH_4 (Y = C,[47] Si,[48] and Ge[49]) molecules, the structure in the angular distributions was partly found in the corresponding noble gas species (Ne, Ar, Kr, and Xe atom). Finally, a close inspection in Fig. 4 shows that there are differences with respect to the magnitude of the depths of the critical minimum, suggesting perhaps that "molecular-like" effects are still playing a role here.

D. Vibrational excitations

Fig. 1 shows the EEL spectra of BF_3 in the vibrational excitation region obtained at the impact energies and scattering angles of 1.5 at 20° and 4.0 eV at 20° with an energy resolution

TABLE I. Elastic differential (10^{-16} cm^2/sr), integral cross sections Q_I and momentum transfer cross sections Q_m (10^{-16} cm^2) for BF_3. Errors on the DCS are typically 10%–15%, on the ICS and MTCS ~30%–33%.

	Energy (eV)													
Angle (deg)	1.5	2.0	3.0	3.5	4.0	5.0	7.0	10	15	20	30	60	100	200
15	…	…	…	…	…	…	1.317	1.934	3.143	7.281	…	…	…	…
20	0.729	0.491	0.893	1.709	1.864	1.239	1.609	2.105	2.754	5.728	…	4.066	1.996	1.330
30	0.559	0.382	0.775	1.455	2.026	1.404	2.103	1.855	1.765	3.235	3.226	0.934	0.806	0.642
40	0.405	0.351	0.840	1.429	2.065	1.479	2.234	1.694	1.170	1.853	1.391	0.674	0.483	0.372
50	0.257	0.356	0.863	1.441	1.774	1.434	1.930	1.388	0.705	1.066	0.766	0.493	0.264	0.267
60	0.322	0.405	0.802	1.404	1.464	1.157	1.218	0.836	0.535	0.730	0.699	0.275	0.204	0.118
70	0.338	0.436	0.879	1.143	1.136	0.742	0.777	0.604	0.548	0.643	0.569	0.191	0.167	0.080
80	0.340	0.416	0.854	1.003	0.908	0.470	0.518	0.539	0.561	0.508	0.422	0.134	0.114	0.073
90	0.385	0.456	0.901	0.893	0.743	0.377	0.404	0.585	0.526	0.401	0.307	0.118	0.078	0.067
100	0.412	0.465	0.820	0.807	0.607	0.346	0.395	0.605	0.397	0.363	0.269	0.111	0.076	0.072
110	0.398	0.447	0.803	0.809	0.632	0.414	0.478	0.539	0.288	0.438	0.304	0.142	0.105	0.070
120	0.430	0.501	0.728	0.826	0.793	0.531	0.554	0.507	0.297	0.606	0.444	0.231	0.161	0.076
130	0.413	0.465	0.773	0.998	1.026	0.628	0.591	0.538	0.525	0.879	0.644	0.299	0.197	0.083
140	…	…	…	…	…	…	…	…	…	…	1.013	0.426	0.249	0.089
150	…	…	…	…	…	…	…	…	…	…	1.336	0.536	…	…
Q_I	5.156	5.212	10.319	14.427	15.083	9.825	11.341	10.580	10.131	15.574	13.333	7.378	4.560	2.881
Q_m	5.025	5.414	10.067	13.251	13.373	7.917	8.225	8.108	8.049	11.493	9.238	3.917	2.495	1.234

of 30–40 meV. Those electron energies were chosen to be close to the R-T minimum and shape resonance, respectively. As mentioned above, in addition to the elastic peak, the spectra reveal the presence of two distinct groups of bands, i.e., the composed modes ($\upsilon_4 + \upsilon_2 + \upsilon_1$) and degenerate stretching, υ_3 mode centered at energy losses of 0.075 eV and 0.180 eV, respectively. BF_3, like CF_4,[44] is one of the few molecules where the υ_3 mode is isolated from the υ_1 mode. For planar molecules such as BF_3, the symmetric stretching υ_1 mode is Raman active and the out-of-plane deformation υ_2 mode is IR active, while the degenerate stretching υ_3 and υ_4 modes are active in both. These features are summarized in Table II. To improve the signal-to-noise ratio, we have integrated these two peaks using Gaussian functions and normalized to the corresponding elastic DCS. The angular distributions of composed ($\upsilon_4 + \upsilon_2 + \upsilon_1$) and υ_3 modes at 1.5, 4.0, and 15 eV obtained from the EELS data such as Fig. 1 are shown in Fig. 5.

At 1.5 eV impact energy and forward scattering angles, the υ_3 mode DCS increases similarly as the elastic DCS. Such behavior has been observed in fluorine containing molecules, e.g., CH_3F,[19] CF_4,[44] C_2F_6,[50] and SF_6[51] for electron impact energy approaching the region of the R-T minimum. Note that although the υ_3 mode excitation is optically forbidden, it is Raman active, whereas in the case of υ_2 and υ_3 modes with large IR activities, direct dipole scattering will produce large vibrational cross sections, in particular, near the threshold. Therefore, at 1.5 eV, the strongly forward peaked angular distributions of υ_3 mode most likely indicate a typical Born-like behavior, i.e., monotonically decreasing function from direct scattering as the scattering angle becomes larger[52] as shown in Fig. 5. The disagreement between the Born-curve and measured DCSs at larger scattering angles in Fig. 5 may be due to limitation of the Born approximation or may indicate the influence from an underlying shape resonance in the vicinity of 3.8 eV. Note that for this feature, the DCS behavior (see Fig. 2) is in contrast to the elastic DCS at 1.5 eV, showing isotropic angular distribution dominated by an s-wave character.

TABLE II. Physical and chemical properties of BF_3.

Symmetry of ground state		A_1'
B-F internuclear distance (a.u.)		2.45
F-B-F angles		120°
Polarizability (Å^3)		3.31
Symmetry species Γ_i	Normal modes (nuclear motion)	Vibrational energy ΔE (eV)	Activity
a_1'	ν_1 (symmetry stretching)	0.110	R
a_2	ν_2 (out of plane-deform)	0.086	IR
e′	ν_3 (degenerate stretching)	0.180	IR, R
e′	ν_4 (degenerate stretching)	0.059	IR, R

Shape resonances reveal strong selectivity in vibrational excitation. The vibrational modes are, in general, obtained by assuming that the operator transforming the initial symmetric vibrational state, ψ_i (Γ_i) to the final vibrational states ψ_f (Γ_f), belongs to the same irreducible representation as the electron density of the temporarily bound state ($\Gamma_{TNI} = \Gamma_L \times \Gamma_L$). The direct product rules for $\langle \psi_f | H | \psi_i \rangle \neq 0$ allow one to calculate the symmetry species of the final states. Γ_e of the outgoing electron-wave can be obtained from $\psi_f \times \Gamma_e = \Gamma_{TNI}$. An expansion of these species into spherical harmonics shows that the electron-wave in the molecular frame has the contribution of three angular momenta.[53] These representations are summarized in Table III for the predicted transient negative ion (TNI) states (Γ_L) corresponding to three D_{3h}, C_{3v}, and C_{2v} point groups, and the symmetry species for the fundamental vibrational modes in Table II. The electronic ground state configuration of BF_3 with symmetry D_{3h} is

$$(1a_1')^2(1e')^4(2a_1')^2(3a_1')^2(2e')^4(4a_1')^2(3e')^4(1a_2'')^2(4e')^4(1e'')^4(1a_2')^2\ {}^1A_1'.$$

However, since BF_3 is a planar molecule, it can also be treated within C_{2v} symmetry, like other planar molecules as F_2CO.[15]

The first study on the vibrational excitation by low energy electron impact in a crossed-beam experiment has been performed by Tronc *et al.*[11] Three broad resonance structures at around 3.8, 10.3, and 13.7 eV were observed in the inelastic vibrational excitations of v_3 ($+2v_2$) and v_1 ($+v_2$) modes at a scattering angle of 90°. From Table III, these broad maxima at 3.8 and 13.7 eV were assigned to shape resonances with a_2'' and e' symmetries, i.e., a molecule in the ground state plus an electron temporally trapped in a low-lying unoccupied molecular orbitals of a_2'' and e' symmetries. A typical resonance enhancement in the vibrational excitation was observed for the v_1 mode. Moreover, the v_2 mode was also enhanced due to the symmetry change from a_2'' (D_{3h}) to a_1 (C_{3v}) of the temporary negative ion, BF_3^-. Such is due to the fact that the energy of the a_2'' orbital decreases as the F-B-F angle changes from 120° to 90°, leading to a pyramidal geometry of C_{3v} symmetry. Therefore, it is reasonable to assume that the predominant pathway for vibrational excitation with the resonant energy occurs by TNI decay, while the bands comprising, v_1, v_2, and v_4 are excited by a breakdown of the optical selection rules, which is due to the low impact energy. Direct scattering is always the inevitable contribution which covers the resonant characteristics, specifically for the elastic scattering.

As discussed briefly above, the feature at 3.8 eV was confirmed at fairly close energy of 3.54 eV in the ETS of Tossel *et al.*,[12] whereas the weak structures in the total cross section from 6 to 14 eV were not reproduced in such ETS experiments. In addition to the ETS, multiple Xα-calculation was carried out to clarify these experimental resonances in which the unoccupied a_2'', a_1', and e' orbitals were assumed to generate the resonances at 3.5 and 13–16 eV, respectively. More recently, the R-matrix of Radmilović-Radjenović *et al.*[13] and the SMC calculation of Pastega *et al.*[15] confirmed the strong resonance with B_1 and B_2 symmetries belonging to the C_{2v} point group, in which the DCSs were also provided for the elastic scattering. In the SEP approximation of the SMC calculation around 3.5 eV and at 10 eV, the elastic DCSs are represented by a shallow p-wave ($l = 1$) and a weak d-wave ($l = 2$) behavior, respectively. There is also a very small indication that $l = 3$ partial wave contributes to the elastic scattering.

TABLE III. Symmetry analysis within the point groups of D_{3h}, C_{3v}, and C_{2v}.

Point group	D_{3h}		C_{3v}	C_{2v}
Ground state	A_1'		A_1	A_1
Γ_L (LUMO)	a_2'', a_1'	e'	a_1	b_2
$\Gamma_{TNI} = \Gamma_L' \Gamma_L$	a_1'	a_1', a_2', e'	a_1	a_1
$\Gamma_{elastic}$	a_1'	a_1', a_2', e'	a_1	a_1
$l_{out-elastic}$	0, 2	0, 1, 2	0, 1	0, 1
Γ_f	a_1'	a_1', a_2', e'	a_1	a_1
ν	ν_1	$\nu_1, \nu_2, \nu_3, \nu_4$	ν_1, ν_2	ν_1, ν_2, ν_3
$\Gamma_{wave-out}$	a_1'	a_1', e'	a_1	a_1
l_{out}	0, 2	0, 2, 1, 2	0, 1	0, 1

However, to our knowledge, no angular distribution of BF_3 has been measured for the vibrational excitations. The present measurement is limited from 1.5 to 15 eV. As clearly shown in Fig. 5, prominent features emerge in the angular distributions of the vibrational excitation functions, which are more enhanced than those in the elastic scattering close to the R-T minimum at 1.5 eV, and near the shape resonances at 4.0 and 15 eV. These DCSs shed light in understanding which angular momentum dominates in the resonant scattering process. The angular momentum contribution of the scattered electron in the molecular frame is shown in Table III, with the angular distributions of the vibrational DCSs, σ (θ) in the laboratory frame must have the following form:[53,54]

$$\sigma(\theta) = \sum_k a_k P_k(\cos\theta) = a_0 + a_1 P_1(\cos\theta) + a_2 P_2(\cos\theta) + \cdots. \quad (1)$$

Here, $P_k(\cos\theta)$ are the Legendre polynomials. The expression contains even and odd orders of Legendre polynomials because both entrance- and exit-channels include even and odd quantum numbers of the angular momenta. In contrast with the elastic DCS at 4.0 eV, the angular distribution for the composed modes reveals weak d-wave ($l = 2$) feature on the isotropic flat-behavior due to an s-wave ($l = 0$) scattering, while the increasing trend of the DCSs still remains towards the forward scattering at 1.5 eV. A bump with minima around 50° and 110° and a slightly hump structure around 80° in the DCS of v_3 mode have appeared as a typical d-wave character, although excitation of v_3 mode is not expected to be relevant due to selection rules of the symmetry analysis in Table III. This feature which is also enhanced more in the v_3 mode at 15 eV supports the requirement of the e' symmetry resonance. At 10 eV, with the exception of the forward peak around 30°, the DCS also becomes isotropic for the composed mode and shows weak d-wave character for v_3 mode, almost the same as at 15 eV (not shown). Consequently, it shows that this broad e' resonant state will couple with the v_3 mode, extending down to around 4 eV.

Fig. 6 shows the angular distributions of vibrational DCSs for resolved vibrational modes at 4 eV. Solid lines represent the angular distributions fitted by the Legendre polynomials of order k in Table III for each mode. Due to the present symmetry analysis,[54] v_1 mode being excited via a shape resonance reveals slightly a broad hump around 90° on the flat angular distribution. If the hump is enhancement due to the shape resonance, the Clebsch-Gordan coefficients, $l + l' - k \geq 0$, restrict the allowed value of l_{out} as shown in Table III. This

result is also evidence that the only resonance fulfilling this condition is either a_2'' or a_1' symmetry with $l_{out} = 0$ or 2.

E. Integral and momentum transfer cross sections: Q_I and Q_m

The integral cross sections, Q_I and particularly Q_m, are essential for use in modeling calculations and plasma simulations. The integrations were carried out by the procedures presented in Sec. III.

Figs. 7(a) and 7(b) show the elastic ICS, Q_I and MTCS, Q_m, derived from the present DCSs and compared with other previous measurements and theoretical results. In Fig. 7(a), in the whole energy range from 1.5 to 200 eV, we find very good agreement between the present TCS, which is the sum of the elastic with the vibrational ICS and the previous TCS measurements of Szmytkowski *et al.*[9] As far as the total inelastic ICS from the IAM-SCAR calculations is concerned, our experimental TCS also agrees very well in the high energy region, i.e., above 20 eV. We observe that the TCS exhibits a structure in the vicinity of the B_2 shape resonance at 3.5–4 eV and decreases for lower impact energies towards the R-T minimum at 0.7 eV.[15] In Fig. 7(a), we also make a comparison between the present elastic ICS, the IAM-SCAR calculations, and previous available data in the literature. The agreement between our data and IAM-SCAR is reasonable above 20 eV, while the most recent calculation (SMC-SEP)[15] reproduces not only the experimental energy dependence at the shape resonance region but also the decreasing behavior for lower impact energies. Such agreement contrasts with other calculations.[12–14] Furthermore, Fig. 7(a) shows the inelastic ICSs for degenerate stretching, υ_3 mode and composed $(\upsilon_1 + \upsilon_2 + \upsilon_4)$ modes together with the total inelastic ICSs from the present IAM-SCAR calculations. BEf-scaled ICSs for the optically allowed transition of $(\pi \rightarrow \pi^*)$ at 13.13 eV were reported more recently[55] by our group and previous ionization cross sections[3,4,10] are also plotted in Fig. 7(a). Note that we observe fairly good agreement between the υ_3 to the $(\upsilon_1 + \upsilon_2 + \upsilon_4)$ ratio of the present ICSs and the excitation function of Tronc *et al.*[11] at 90°. Also, reasonable agreement is observed between our ICS and partial cross section for υ_3 mode derived from swarm data,[1] whereas the present $(\upsilon_1 + \upsilon_2 + \upsilon_4)$ vibrational-sum ICS differs from the swarm data[1] (not shown).

In Fig. 7(b), we present the elastic MTCS, Q_m together with the recent calculations from SMC-SE and SEP[15] methods and those derived from swarm data.[1] We find fairly good agreement between our data and the results of the SMC-SEP calculation[15] in the whole energy region. The energy dependence of Q_m derived from swarm experiment[1] agrees with the present Q_m below 5 eV, whereas there is still a discrepancy in the higher energy region.

V. CONCLUSIONS

We report experimental elastic differential, integral, and momentum transfer cross sections for electron scattering from BF_3 molecules in the energy range from 1.5 to 200 eV and at the scattering angle range from 15° to 150°. In addition, corresponding IAM-SCAR formulation was also performed to compare against our measurements. These results, particularly for electron energy above 20 eV, were found to be in good quantitative agreement with the present elastic DCS data, whereas below 20 eV, the experimental DCSs agree with the SMC-SEP calculation reported recently. Comparison with other three-fluorine containing molecules, XF_3 (X = B, C, N, and CH), and calculated DCS from IAM-SCAR model for these molecular systems and atomic fluorine have also been discussed. From these comparisons, agreement between these sets of data is generally very good for BF_3, NF_3, and CHF_3 above 30 eV electron impact energies, but an inexplicable factor of 10 difference was found for DCSs of the CF_3 radical at 7.0 eV. The level of agreement reported here suggests that atomic-like behavior in the scattering processes may be of considerable relevance, at least in the energy range above 30 eV, which is similar to the other scattering systems such as CCl_4, YF_4 (Y = C, Si, and Ge), COS and CS_2, and C_nF_6 (n = 2, 3, 4, and 6) targets reported recently. Integral elastic and vibrational cross sections were determined and found to be in reasonable good agreement with the results from not only the present IAM-SCAR but also SMC-SEP calculations.

We performed vibrational analysis using the angular correlation theory and found that the only shape resonance fulfilling this condition has either a_2'' or a_1' symmetry. Finally, the total cross sections summed elastic ICS with inelastic ICS were also found to be nicely consistent with the previous results from TCS measurements of Szmytkowski *et al.*[9]

ACKNOWLEDGMENTS

This work was conducted under the support of the Japanese Ministry of Education, Sport, Culture, and Technology. F.F.S. acknowledges the Portuguese Foundation for Science and Technology (FCT-MEC) for post-doctoral No. SFRH/BPD/68979/2010 grant, and together with PL-V the Nos. UID/FIS/00068/2013 and PTDC/FIS-ATO/1832/2012 grants through FCT-MEC. PL-V also acknowledges his Visiting Professor position at Sophia University, Tokyo, Japan. F.B. and G.G. acknowledge the partial financial support from the Spanish Ministerio de Economia y Competitivided (Project No. FIS 2012-31230).

[1] P. X. Hien, B.-H. Jeon, and D. A. Tuan, J. Phys. Soc. Jpn. **82**, 034301 (2013).
[2] V. D. Stojanovic, Z. M. Raspopovic, J. V. Jovanovic, S. B. Radovanov, Z. D. Nikitovic, and Z. Lj. Petrovic, Nucl. Instrum. Methods Phys. Res., Sect. B **279**, 151 (2012).
[3] M. V. Kurepa, V. M. Pejcev, and I. M. Cadez, J. Phys. D **9**, 481 (1976).
[4] Y.-K. Kim and K. K. Irikura, AIP Conf. Proc. **543**, 220 (2000).
[5] K. A. MacNeil and J. C. J. Thynne, J. Phys. Chem. **74**, 2257 (1970).
[6] J. J. DeCorpo and J. L. Frankline, J. Chem. Phys. **54**, 1885 (1971).
[7] J. A. Stockdale, D. R. Nelson, F. J. Davis, and R. N. Compton, J. Chem. Phys. **56**, 3336 (1972).
[8] P. W. Harland and J. L. Frankline, J. Chem. Phys. **61**, 1621 (1974).
[9] C. Szmytkowski, M. Piotrowicz, A. Domaracka, L. Klosowski, E. Ptasinska-Denga, and G. Kasperski, J. Chem. Phys. **121**, 1790 (2004).
[10] M. Vinodkumar, K. Korot, C. Limbachiya, and B. K. Antony, J. Phys. B: At., Mol. Opt. Phys. **41**, 245202 (2008).
[11] M. Tronc, L. Malegat, R. Azria, and Y. LeCoat, J. Phys. B: At., Mol. Opt. Phys. **15**, L253 (1982).
[12] J. A. Tossell, J. H. Moore, and J. K. Olthoff, Int. J. Quantum Chem. **29**, 1117 (1986).
[13] M. Radmilović-Radjenović, H. N. Varambhia, M. Vranić, J. Tennyson, and Z. Lj. Petrović, Publ. Astron. Obs. Belgrade **84**, 57 (2008).

[14]R. F. da. Costa, L. G. Ferreira, M. A. P. Lima, and M. H. F. Bettega, J. Chem. Phys. **118**, 75 (2003).
[15]D. F. Pastega, R. F. Da Costa, M. A. P. Lima, and M. H. F. Bettega, Eur. Phys. J. D **68**, 20 (2014).
[16]L. Boesten, Y. Tachibana, Y. Nakano, T. Shinohara, H. Tanaka, and M. A. Dillon, J. Phys. B: At., Mol. Opt. Phys. **29**, 5475 (1996).
[17]T. N. Rescigno, Phys. Rev. A **52**, 329 (1995).
[18]E. Joucoski and M. H. F. Bettega, J. Phys. B: At., Mol. Opt. Phys. **35**, 783 (2002).
[19]T. Marcio, N. Varella, C. Winstead, V. McKoy, M. Kitajima, and H. Tanaka, Phys. Rev. A **65**, 022702 (2002).
[20]J. R. Brunton, L. R. Hargreaves, S. J. Buckman, G. García, F. Blanco, O. Zatsarinny, K. Bartschat, and M. J. Brunger, Chem. Phys. Lett. **55**, 568-569 (2013).
[21]J. R. Brunton, L. R. Hargreave, T. M. Maddern, S. J. Buckman, G. Garcia, F. Blanco, O. Zatsarinny, K. Bartschat, D. B. Jones, G. B. da. Silva, and M. J. Brunger, J. Phys. B: At., Mol. Opt. Phys. **46**, 245203 (2013).
[22]F. Blanco and G. García, Phys. Lett. **360**, 707 (2007).
[23]F. Blanco, J. Rosado, A. Illana, and G. García, Phys. Lett. A **374**, 4420 (2010).
[24]H. Kato, T. Asahina, H. Masui, M. Hoshino, H. Tanaka, H. Cho, O. Ingolfsson, F. Blanco, G. Garcia, S. J. Buckman, and M. J. Brunger, J. Chem. Phys. **132**, 074309 (2010).
[25]P. Limão-Vieira, M. Horie, H. Kato, M. Hoshino, F. Blanco, G. García, S. J. Buckman, and H. Tanaka, J. Chem. Phys. **135**, 234309 (2011).
[26]H. Kato, A. Suga, M. Hoshino, F. Blanco, G. García, P. Limão-Vieira, M. J. Brunger, and H. Tanaka, J. Chem. Phys. **136**, 134313 (2012).
[27]H. Kato, K. Anzai, T. Ishihara, M. Hoshino, F. Blanco, G. García, P. Limão-Vieira, M. J. Brunger, S. J. Buckman, and H. Tanaka, J. Phys. B: At., Mol. Opt. Phys. **45**, 095204 (2012).
[28]H. Murai, Y. Ishijima, T. Mitsumura, Y. Sakamoto, H. Kato, M. Hoshino, F. Blanco, G. García, P. Limão-Vieira, M. J. Brunger, S. J. Buckman, and H. Tanaka, J. Chem. Phys. **138**, 054302 (2013).
[29]M. Hoshino, P. Limão-Vieira, K. Anzai, H. Kato, H. Cho, D. Mogi, T. Tanioka, F. Ferreira da Silva, D. Almeida, F. Blanco, G. García, O. Ingólfsson, and H. Tanaka, J. Chem. Phys. **141**, 124302 (2014).
[30]H. Tanaka, L. Boesten, D. Matsunaga, and T. Kudo, J. Phys. B: At., Mol. Opt. Phys. **21**, 1255 (1988).
[31]H. Tanaka, T. Ishikawa, T. Masai, T. Sagara, L. Boesten, M. Takekawa, Y. Itikawa, and M. Kimura, Phys. Rev. A **57**, 1798 (1998).
[32]T. Shimanouchi, J. Phys. Chem. Ref. Data **6**, 1010 (1977).
[33]S. F. Wong and A. L. Dube, Phys. Rev. A **17**, 570 (1978).
[34]L. Boesten and H. Tanaka, At. Data Nucl. Data Tables **52**, 25 (1992).
[35]S. K. Srivastava, A. Chutian, and S. Trajmar, J. Chem. Phys. **63**, 2659 (1975).
[36]R. T. Brinkmann and S. Trajmar, Rev. Sci. Instrum. **14**, 245 (1981).
[37]S. Trajmar and D. F. Register, in *Electron-Molecule Collisions*, edited by I. Shimamura and K. Takayagi (Plenum, New York, 1984), pp. 427–493.
[38]J. C. Nikel, P. W. Zetner, G. Shen, and S. Trajmar, J. Phys. E: Sci. Instrum. **22**, 730 (1989).
[39]F. Rugamas, D. Roundy, G. Mikaelian, G. Vitug, M. Rudner, J. Shih, D. Smith, J. Segura, and M. A. Khakoo, Meas. Sci. Technol. **11**, 1750 (2000).
[40]M. A. Dillon, L. Boesten, H. Tanaka, M. Kimura, and H. Sato, J. Phys. B: At., Mol. Opt. Phys. **27**, 1209 (1994).
[41]H. Tanaka, T. Okada, L. Boesten, T. Suzuki, T. Yamamoto, and M. Kudo, J. Phys. B: At., Mol. Opt. Phys. **15**, 3305 (1982).
[42]D. G. Thompson, J. Phys. B: At., Mol. Opt. Phys. **4**, 468 (1971).
[43]G. G. Raju, IEEE Trans. Dielectr. Electr. Insul. **16**, 1199 (2009).
[44]L. Boesten, H. Tanaka, A. Kobayashi, M. A. Dillon, and M. Kimura, J. Phys. B: At., Mol. Opt. Phys. **25**, 1607 (1992).
[45]R. B. Diniz, M. A. P. Lima, and F. J. da. Paixão, J. Phys. B: At., Mol. Opt. Phys. **32**, L539 (1999).
[46]I. Rozum and J. Tennyson, J. Phys. B: At., Mol. Opt. Phys. **37**, 957 (2004).
[47]L. Boesten and H. Tanaka, J. Phys. B: At., Mol. Opt. Phys. **24**, 821 (1991).
[48]H. Tanaka, L. Boesten, H. Sato, M. Kimura, M. A. Dillon, and D. Spence, J. Phys. B: At., Mol. Opt. Phys. **23**, 577 (1990).
[49]M. A. Dillon, L. Boesten, H. Tanaka, M. Kimura, and H. Sato, J. Phys. B: At., Mol. Opt. Phys. **26**, 4075 (1993).
[50]T. Takagi, L. Boesten, H. Tanaka, and M. A. Dillon, J. Phys. B: At., Mol. Opt. Phys. **27**, 5389 (1994).
[51]H. Cho, R. J. Gulley, K. W. Trantham, L. J. Uhlmann, C. J. Dedman, and S. J. Buckman, J. Phys. B: At., Mol. Opt. Phys. **33**, 3531 (2000).
[52]Y. Itikawa, Phys. Rev. A **3**, 831 (1971).
[53]F. H. Read, J. Phys. B: At., Mol. Opt. Phys. **1**, 892 (1968).
[54]D. Andrick and F. H. Read, J. Phys. B: At., Mol. Opt. Phys. **4**, 389 (1971).
[55]D. Duflot, M. Hoshino, P. Limao-Vieira, A. Suga, H. Kato, and H. Tanaka, J. Phys. Chem. A **118**, 10955 (2014).